# MedChemComm

Broadening the field of opportunity for medicinal chemists

www.rsc.org/medchemcomm

Volume 4 | Number 10 | October 2013 | Pages 1315–1414

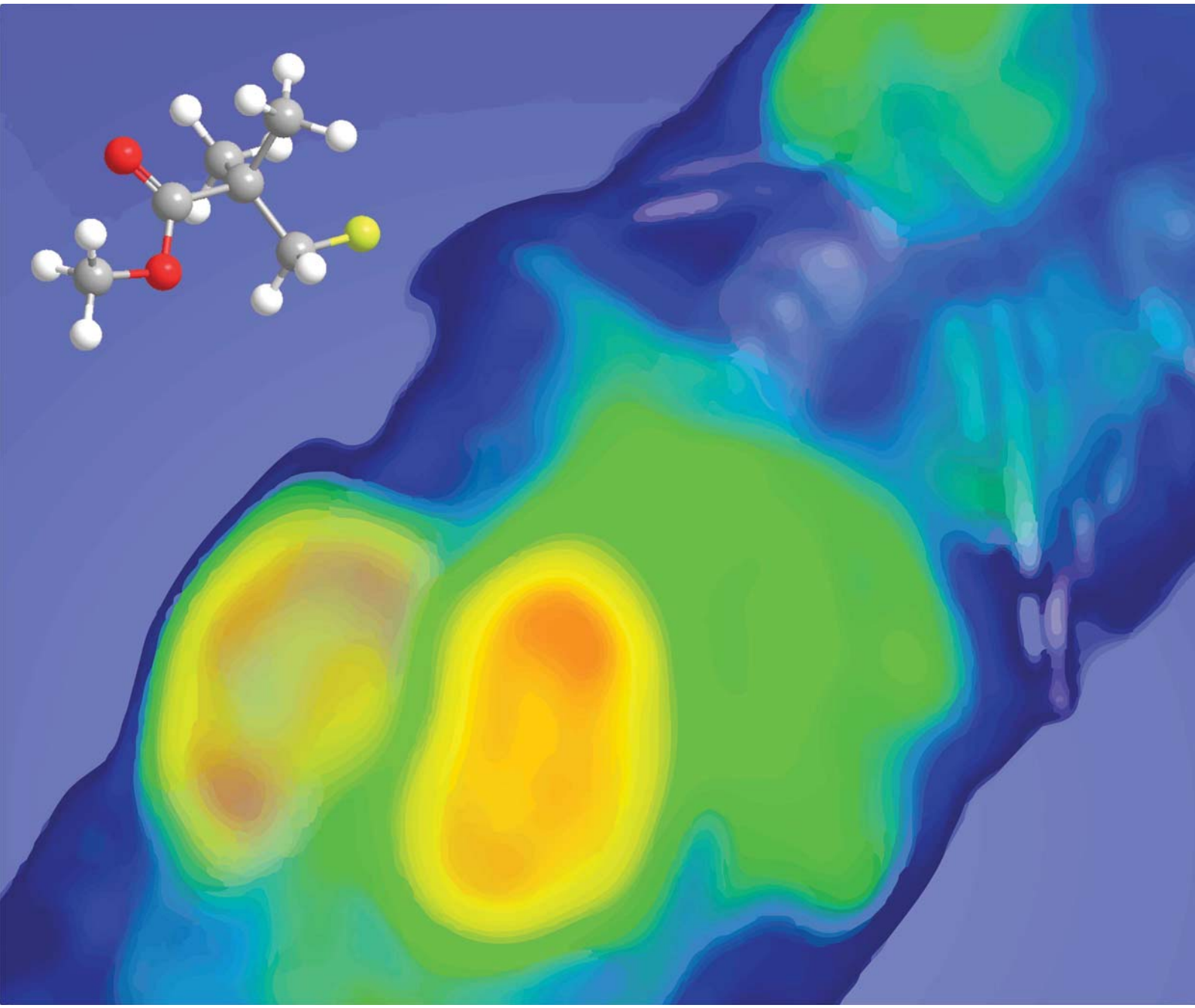

ISSN 2040-2503

**CONCISE ARTICLE**

Federica Pisaneschi *et al.*

Synthesis of [$^{18}$F]fluoro-pivalic acid: an improved PET imaging probe for the fatty acid synthesis pathway in tumours

RSC Publishing

EFMC European Federation for Medicinal Chemistry

2040-2503(2013)4:10;1-1

MedChemComm

RSC Publishing

CONCISE ARTICLE

View Article Online
View Journal | View Issue



**Cite this:** *Med. Chem. Commun.*, 2013, **4**, 1350

Received 13th June 2013
Accepted 16th July 2013

DOI: 10.1039/c3md00169e

**www.rsc.org/medchemcomm**

# Synthesis of [$^{18}$F]fluoro-pivalic acid: an improved PET imaging probe for the fatty acid synthesis pathway in tumours†

Federica Pisaneschi,‡* Timothy H. Witney,‡ Lisa Iddon‡ and Eric O. Aboagye

[$^{18}$F]Fluoro-pivalic acid ([$^{18}$F]FPIA), an analogue of [$^{18}$F]fluoroacetate bearing a dimethyl moiety on C-2, has been radiosynthesised and evaluated *in vivo*. [$^{18}$F]FPIA has high tumour uptake and, unlike [$^{18}$F]fluoroacetate, does not defluorinate.

Prostate cancer is the most prevalent of cancers in the male population, accounting for 40 841 incidents in the UK in 2009.[1] In the USA prostate cancer is the second largest cause of cancer mortality amongst men. Positron emission tomography (PET) is routinely used in the clinic for cancer detection, with the majority of all scans performed with the glucose analogue [$^{18}$F]-2-fluoro-2-deoxyglucose, [$^{18}$F]FDG. A number of clinical studies, however, have shown poor sensitivity for prostate cancer detection by [$^{18}$F]FDG-PET, resulting from low basal glucose metabolism of some prostate tumours[2] and the high renal clearance of [$^{18}$F]FDG, which can often mask tumour uptake.[3] As a result, other PET tracers have been developed for prostate cancer imaging such as [$^{11}$C]choline, [$^{18}$F]fluorocholine and [$^{11}$C]acetate.

[$^{11}$C]Acetate was initially developed as a radiotracer to evaluate oxidative metabolism in the myocardium. Following entry into the cell, either by passive diffusion or membrane transport *via* the monocarboxylate transporters,[4] [$^{11}$C]acetate is converted to [$^{11}$C]acetyl-CoA by acetyl-CoA synthetase before its rapid metabolism *via* the citric acid cycle to [$^{11}$C]$CO_2$.[5] As well as being a substrate for the citric acid cycle, acetyl-CoA also contributes to *de novo* fatty acid synthesis, with tumour-associated [$^{11}$C]-acetate accumulation shown to result from cell membrane incorporation following flux through the fatty acid synthesis pathway. Experiments carried out by Yoshimoto and co-workers showed that [1-$^{14}$C]acetate was incorporated into the lipid soluble fraction, mostly as phosphatidylcholine and neutral lipids. The accumulation of [1-$^{14}$C]acetate was positively correlated with the growth of the tumour cells. Fatty acid synthase (FAS) has been shown to be overexpressed in tumours, contributing to elevated acetate uptake and incorporation into the cell membrane.[6,7] Furthermore, Yoshii and co-workers reported that tumour uptake of acetate reflects cytosolic acetyl-CoA synthetase,[8] an enzyme that is regulated in part by the fatty acid content.

[$^{11}$C]Acetate has shown promise for prostate cancer imaging,[9] however the short half life of carbon-11 (20.4 min) requires an on-site cyclotron, limiting its wide-spread use. [$^{18}$F]-Fluoroacetate ([$^{18}$F]FAC) was developed by Sykes *et al.*[10] and investigated as an alternative to [$^{11}$C]acetate for imaging of prostate cancer by Welch and co-workers.[11] The advantage of using fluorine-18 is its longer half life of 109.5 min compared to carbon-11. The authors investigated the biodistribution of [$^{11}$C]-acetate and [$^{18}$F]FAC in Sprague-Dawley rats. They found fairly rapid clearance of [$^{11}$C]acetate from most of the organs except the pancreas at 1 h, perhaps due to the oxidative metabolism of [$^{11}$C]acetate, releasing [$^{11}$]$CO_2$, whereas [$^{18}$F]FAC clearance was slower from most organs. The main drawback of [$^{18}$F]FAC is its substantial bone uptake, characteristic of radiotracer defluorination.[11] There are a number of putative routes for defluorination (Scheme 1). Tecle and Casida,[12] for example, found that

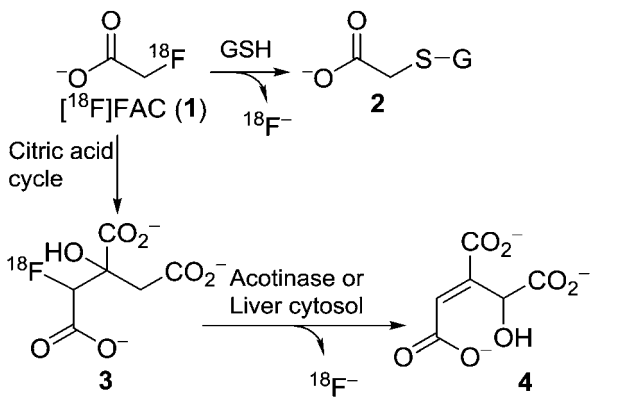


**Scheme 1** Mechanisms of [$^{18}$F]FAC defluorination.

*Comprehensive Cancer Imaging Centre, Department of Surgery and Cancer, Imperial Centre for Translational and Experimental Medicine, Hammersmith Hospital, Du Cane Road, London W12 0NN, UK. E-mail: f.pisaneschi@imperial.ac.uk; Tel: +44 (0) 20 3313 3204*

† Electronic supplementary information (ESI) available. See DOI: 10.1039/c3md00169e

‡ These authors contributed equally to this work.

incubation of [$^{13}$C]fluoroacetate with rat and mouse liver cytosol led to defluorination, with fluoride ion displacement resulting from nucleophilic attack by glutathione (GSH). [$^{18}$F]FAC also undergoes defluorination *via* its metabolism in the citric acid cycle. Once [$^{18}$F]FAC enters the citric acid cycle, it is converted into 2-fluorocitrate **3**. The same authors,[12] together with other groups[13,14] showed that (−)-*erythro*-2-fluorocitrate **3** is further converted to fluoro-*cis*-aconitate by aconitase, undergoing addition of hydroxide and subsequent loss of fluoride to form 4-hydroxy-*trans*-aconitate **4**. Compound **4** binds very tightly to the enzyme and it is responsible for the toxicity of fluoroacetate at pharmacological levels. Of note, evidence of defluorination has been found in rodents and pigs, although the rate of defluorination was reduced in non-human primates.[15,16]

Given the inadequate performance of [$^{18}$F]FAC as a tracer that can be used to image biology of acetate metabolism pre-clinically in prostate cancer and beyond, there is a requirement to find a stable imaging agent which does not undergo defluorination.

## Results and discussion

Herein we describe the synthesis of a novel analogue for imaging of acetate metabolism. The criteria for a new analogue was that it should be stable to defluorination in rodents, but still show good uptake in tumour cell lines with increased fatty acid metabolism. An acetate analogue, [$^{18}$F]fluoro-pivalic acid ([$^{18}$F]FPIA, **5**, Fig. 1), also called 3-[$^{18}$F]fluoro-2,2-dimethyl propionic acid, was selected, as it was hypothesised that the *gem*-dimethyl group would prevent this compound from entering the citric acid cycle, not being a substrate for citrate synthase (Fig. 1), thought to contribute to defluorination and slow background clearance from other organs. It was also proposed that [$^{18}$F]FPIA would be slightly less reactive towards glutathione attack due to the inductive effect of the *gem*-dimethyl group and the increased distance of the carboxylic acid.

[$^{18}$F]FPIA is, however, hypothesised to have the capacity to map the initial step of the fatty acid synthesis pathway because it has the potential to be converted into an acetyl-CoA derivative. This would be analogous to the use of [$^{18}$F]fluorodeoxyglucose to map glucose metabolic flux by tumour cells. The synthesis of [$^{18}$F]fluoroacetate is generally carried out using a precursor protected as a methyl or ethyl ester. Ponde *et al.* purified the ester intermediate using a HLB cartridge method. We initially rationalised the synthesis of a FPIA precursor to involve a non-base sensitive carboxylic acid protecting group such as *p*-methoxybenzyl ester that would be stable during the aqueous dilution of the reaction before preparative HPLC. The commercially available 3-bromo-2,2-dimethylpropionic acid **6** was used in a Mitsunobu reaction with 4-methoxybenzyl alcohol. The reaction gave no desired product. A reaction was then attempted using HBTU to form the activated ester, in the presence of DBU. This showed evidence of the desired product but was difficult to separate from the 4-methoxybenzyl alcohol and other by-products. We suspected that the bromine atom competed in the reaction (Scheme 2).

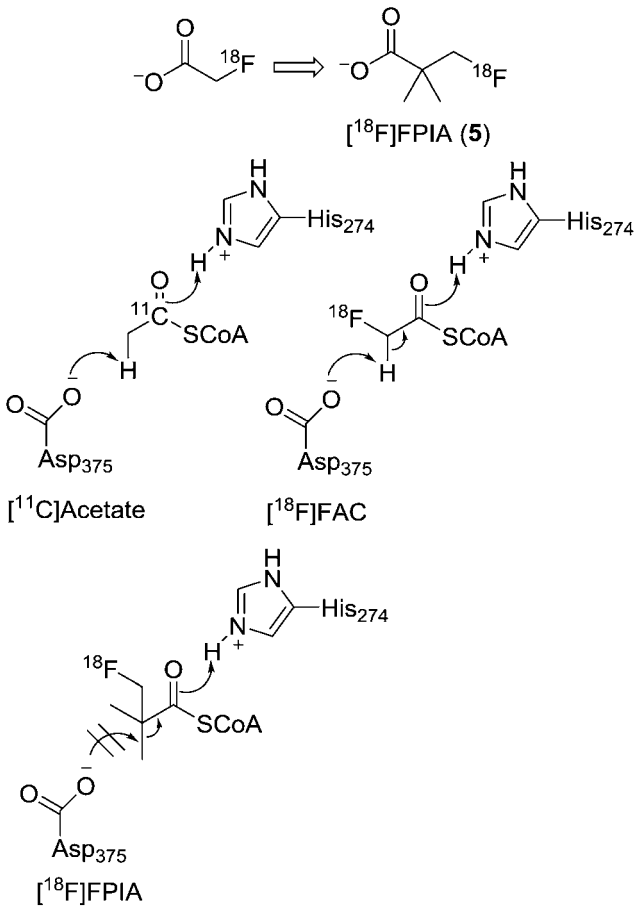


**Fig. 1** Citrate synthase mechanism: first step. The previously published mechanism for entry of acetate into the citric acid cycle[17] has been adapted for [$^{11}$C] acetate, [$^{18}$F]FAC and [$^{18}$F]FPIA. The lack of a proton $\alpha$ to the carbonyl prevents Asp375 from attacking [$^{18}$F]FPIA, disabling the compound from entering the citric acid cycle.

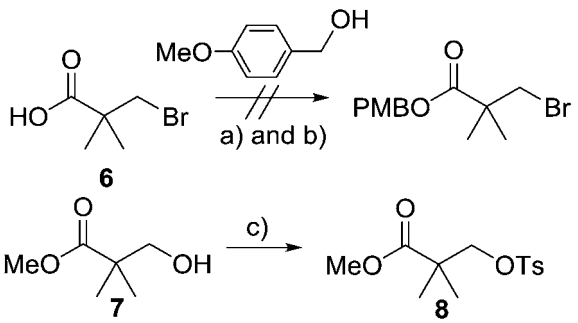


**Scheme 2** *Reagents and conditions*: (a) $PPh_3$, DIAD, THF, 0 °C. (b) HBTU, DBU, $CH_2Cl_2$, rt. (c) TsCl, DMAP, pyridine, rt (70%).

We therefore decided to exploit the methyl ester protecting group strategy as shown by Ponde *et al.*[11] To synthesise a suitable methyl ester protected precursor, methyl 2,2-dimethyl-3-hydroxypropionate (7) was utilised. The hydroxyl group was converted to the tosylate leaving group in good yield (70%) (Scheme 2). The precursor **8** was then taken forward for radiochemistry. Initial experiments to incorporate fluorine-18 were

carried out using $K_2CO_3$ and kryptofix to form the $K^{18}F$/kryptand complex, followed by addition of the precursor in acetonitrile at 80 °C. The reaction was monitored by analytical HPLC. These conditions gave a mixture of radiolabelled products after 5 minutes and only 6% product; further heating led to decomposition of the precursor and only 12% product [$^{18}$F]**9**. The reaction was then undertaken using DMF as solvent at 105 °C, and this showed a robust reaction, giving the product [$^{18}$F]**9** (up to 75% of radiolabel incorporation) and [$^{18}$F]toluenesulfonyl fluoride (25% yield) as a by-product after 15 minutes. At this temperature the precursor was degraded to give methyl-3-hydroxy-2,2-dimethylpropionate. The intermediate was then isolated using reverse phase preparative HPLC and 30% ethanol/water as the eluent. The yield of the isolated compound was remarkably lower than expected from the ratio of conversion. It was suspected that on dilution of the reaction mixture with water, hydrolysis of the methyl ester had occurred giving the final desired product [$^{18}$F]FPIA. The product could not be isolated as it co-eluted at the solvent front with the DMF and any un-reacted fluoride-18. Due to hydrolysis, the isolated yield of the methyl ester intermediate [$^{18}$F]**9** was lower than anticipated (13.9 ± 9.1% decay corrected, $n = 7$). As a less basic environment should disfavour the hydrolysis of the methyl ester, $KHCO_3$ was employed instead of $K_2CO_3$ to form the kryptand complex. The optimal reaction conditions were found to be heating at 110 °C for 10 min. No other radiochemical peaks apart from that for the desired product were observed. This gave up to 80% of incorporation of the fluoride as shown by analytical HPLC (40% MeOH/water) and improved the yield of the isolated product to 39.3 ± 12.6% ($n = 5$) decay corrected (Scheme 3).

Good results were also obtained when [$^{18}$F]TBAF was used as the source of fluoride. The fluoride was dried in the presence of tetrabutylammonium hydrogen carbonate ($TBAHCO_3$) to give [$^{18}$F]TBAF. The use of the less basic $TBAHCO_3$ led to reduced hydrolysis before preparative HPLC. Analysis of the reaction mixture showed complete incorporation of fluoride to give the desired product. After addition of water to the reaction mixture, the preparative HPLC showed 44% product [$^{18}$F]**9** and 52% of the hydrolysed final product, together with unreacted fluorine-18. The methyl ester protected intermediate [$^{18}$F]**9** was isolated in 37% decay corrected yield.

Once isolated from the HPLC eluent, the product was hydrolysed using NaOH (1 M) in 5 min at 60 °C which was then neutralised with HCl (1 M) and phosphate buffered saline was added to achieve a pH of 7.4 and 10% EtOH/PBS or less. The compound identity was proved by co-elution with the cold reference compound FPIA (220 nM). In aggregate, the entire synthesis and formulation takes 1.5 h and delivers [$^{18}$F]FPIA ready for injection in the end of synthesis (EOS) yield of 11.3.± 4.1% ($n = 4$) and >99% radiochemical purity. Accurate and reliable measurement of specific activity was not possible by HPLC due to low UV absorbance of FPIA (see the ESI†). The synthesis was optimised manually with ~750 MBq starting activity. Transfer to an automated platform is currently under investigation.

[$^{18}$F]FPIA pharmacokinetics were tested *in vivo* in non-tumour bearing mice by PET imaging (Fig. 2). Substantial uptake was observed in the cortex of the kidney, with clearance primarily *via* urinary excretion. Tracer localisation was also observed in the heart, liver and intestines. Notably, there was a lack of bone-associated radioactivity, suggesting the absence of (or low) defluorination. A similar radiotracer biodistribution has been previously observed with [$^{11}$C]acetate,[15] except for the route of excretion: elimination *via* [$^{11}$C]$CO_2$ for [$^{11}$C]acetate and *via* the renal route (kidney and urine) for [$^{18}$F]FPIA.

Dynamic [$^{18}$F]FPIA-PET imaging was next performed in BALB/c mice bearing EMT6 murine breast adenocarcinoma xenografts (Fig. 3). In this proof-of-concept study, *in vivo* imaging of implanted EMT6 xenografts showed rapid tumour labelling and retention, with good target : background signal measured 30–60 min post-injection (Fig. 3A and B).

Intracellular EtOH is rapidly catabolised to acetate, which, at high levels, was predicted to compete with the formation of [$^{18}$F]FPIA-CoA and therefore tumour trapping. Tumour-associated radioactivity was increased following EtOH removal

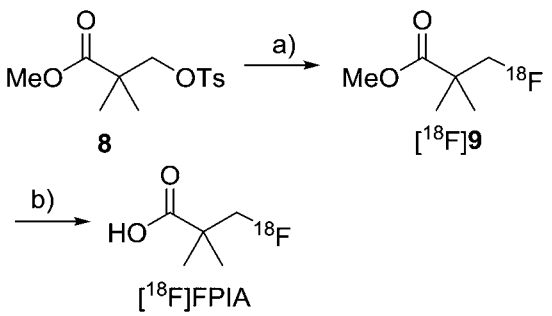


**Scheme 3** Synthesis of [$^{18}$F]FPIA. *Reagents and conditions*: (a) $K_2CO_3$, $K_{222}$, [$^{18}$F]$F^-$ or $KHCO_3$, $K_{222}$, [$^{18}$F]$F^-$ or [$^{18}$F]TBAF, 105–110 °C, 10 min. (b) NaOH (1 M), 60 °C, 5 min, then HCl (1 M) and PBS.

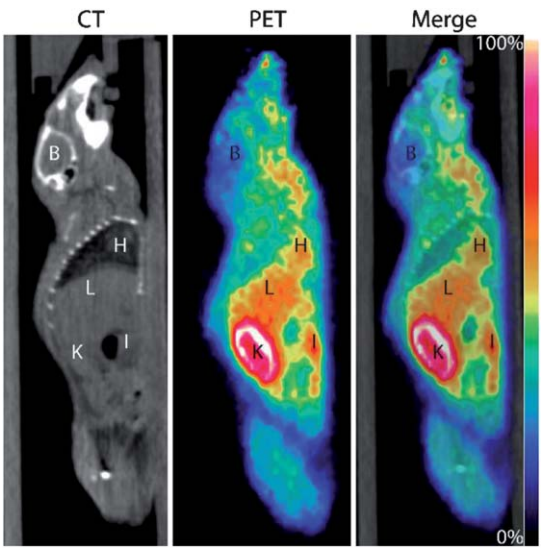


**Fig. 2** PET imaging with [$^{18}$F]FPIA. Representative sagittal CT, PET and PET-CT images (30–60 min summed-activity) for [$^{18}$F]FPIA. Key organs are identified. Abbreviations: B, brain; H, heart; L, liver; K, kidney; I, intestines.

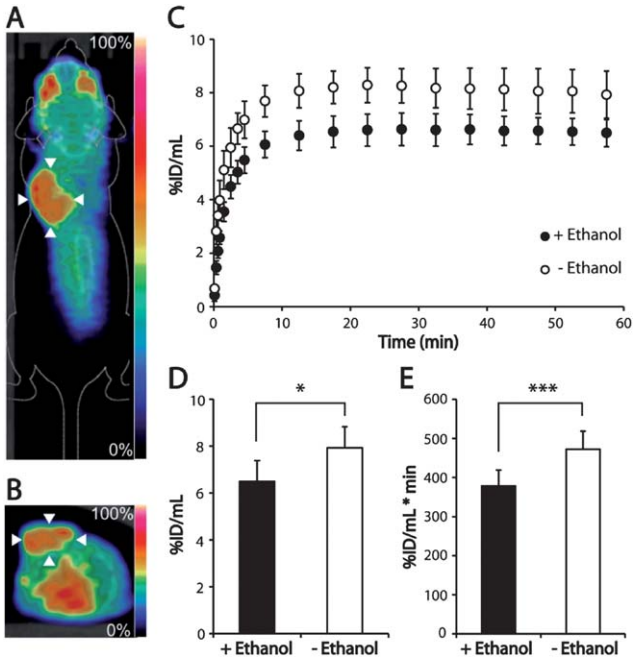


**Fig. 3** Dynamic [$^{18}$F]FPIA PET imaging in EMT6 xenografts. Representative coronal (A) and axial (B) PET-CT images (30–60 min summed-activity) for [$^{18}$F]FPIA. White arrowheads indicate the tumour, identified from the CT image. (C) EMT6 tumour time *versus* radioactivity curve (TAC) obtained from 60 minute dynamic PET imaging with and without EtOH in the final prep. Mean ± SD ($n$ = 4–6 mice per group). (D and E) Semi-quantitative imaging variables extracted from the TAC: tumour radioactivity 60 min post-injection (D) and area under the TAC, 0–60 min (E). Mean ± SD ($n$ = 4–6 mice per group).

of the final prep by heating at 45 °C under vacuum and a stream of nitrogen, shown by the time *versus* radioactivity curves (TAC; Fig. 3C). A significant 1.2-fold increase in tumour radioactivity was measured following EtOH removal at 60 min post-injection, rising from 6.49 ± 0.51% ID mL$^{-1}$ to 7.92 ± 0.88% ID mL$^{-1}$ ($P$ = 0.011; Fig. 3D). Furthermore, a 1.2-fold increase in [$^{18}$F]-FPIA was also measured in EMT6 xenografts over the entire 60 minute time course following EtOH removal, defined by the area under the TAC, increasing from 378 ± 30% ID mL$^{-1}$ min$^{-1}$ to 472 ± 40% ID mL$^{-1}$ min$^{-1}$ ($P$ = 0.0029; Fig. 3E). Although the metabolic fate of [$^{18}$F]FPIA is yet to be experimentally determined, [$^{18}$F]FPIA shows great promise as a cancer imaging agent. Future work will determine its mode of action and provide further biological characterisation.

## Conclusions

A new fluorine-18 labelled tracer, [$^{18}$F]FPIA, analogue of the known [$^{18}$F]FAC, has been designed to potentially image acetate metabolism and the related fatty acid pathway, overexpressed in certain types of cancer. The radiosynthesis involving two steps and one HPLC purification step has been successfully performed in the EOS yield of 11.3 ± 4.1% ($n$ = 4). A key design goal to avoid defluorination was achieved. Preliminary *in vivo* PET imaging showed no bone uptake and high tumour uptake in EMT6 tumour-bearing mice. These encouraging results have prompted further biological evaluation of the radiotracer to assess its potential for the imaging of elevated *de novo* fatty acid synthesis.

## Notes and references

1 http://info.cancerresearchuk.org/cancerstats/types/prostate/incidence/.
2 A. H. Hou, K. F. Sullivan and E. D. Crawford, *Curr. Opin. Urol.*, 2009, **19**, 283–289.
3 R. Wahl, J. Harney, G. Hutchins and H. Grossman, *J. Urol.*, 1991, **146**, 1470–1474.
4 R. A. Waniewski and D. L. Martin, *J. Neurosci.*, 1998, **18**, 5225–5233.
5 R. R. Wolfe and F. Jahoor, *Am. J. Clin. Nutr.*, 1990, **51**, 248–252.
6 F. P. Kuhajda, *Nutrition*, 2000, **16**, 202–208.
7 S. J. Kridel, W. T. Lowther and C. W. Pemble, *Expert Opin. Invest. Drugs*, 2007, **16**, 1817–1829.
8 Y. Yoshii, A. Waki, T. Furukawa, Y. Kiyono, T. Mori, H. Yoshii, T. Kudo, H. Okazawa, M. J. Welch and Y. Fujibayashi, *Nucl. Med. Biol.*, 2009, **36**, 771–777.
9 C. Schiepers, S.-C. Huang and M. Dahlbom, *J. Nucl. Med.*, 2013, **54**, 326.
10 T. R. Sykes, T. J. Ruth and M. J. Adam, *Int. J. Radiat. Appl. Instrum., Part B*, 1986, **13**, 497–500.
11 D. E. Ponde, C. S. Dence, N. Oyama, J. Kim, Y.-C. Tai, R. Laforest, B. A. Siegel and M. J. Welch, *J. Nucl. Med.*, 2007, **48**, 420–428.
12 B. Tecle and J. E. Casida, *Chem. Res. Toxicol.*, 1989, **2**, 429–435.
13 H. Lauble, M. C. Kennedy, M. H. Emptage, H. Beinert and C. D. Stout, *Proc. Natl. Acad. Sci. U. S. A.*, 1996, **93**, 13699–13703.
14 J. J. Villafranca and E. Platus, *Biochem. Biophys. Res. Commun.*, 1973, **55**, 1197–1207.
15 Ö. Lindhe, A. Sun, J. Ulin, O. Rahman, B. Långström and J. Sörensen, *Eur. J. Nucl. Med. Mol. Imaging*, 2009, **36**, 1453–1459.
16 R. Nishii, W. Tong, R. Wendt, III, S. Soghomonyan, U. Mukhopadhyay, J. Balatoni, O. Mawlawi, L. Bidaut, P. Tinkey, A. Borne, M. Alauddin, C. Gonzalez-Lepera, B. Yang and J. Gelovani, *Mol. Imaging Biol.*, 2012, **14**, 213–224.
17 G. Wiegand and S. J. Remington, *Annu. Rev. Biophys. Biophys. Chem.*, 1986, **15**, 97–117.